

# Design and Performance of the ICON EUV Spectrograph

Martin M. Sirk\*, Eric J. Korpela, Yuzo Ishikawa, Jerry Edelsetin, Edward H. Wishnow, Christopher Smith, Jeremy McCauley, Jason B. McPhate, James Curtis, Travis Curtis, Steven R. Gibson, Sharon Jelinsky<sup>a</sup>, Jeff Lynn, Mario Marckwordt, Nathan Miller, Michael Raffanti, William Van Shourt, Andrew W. Stephan<sup>b</sup> and Thomas Immel

University of California, Space Sciences Laboratory, Berkeley CA, USA

<sup>a</sup>Lawrence Berkeley National Laboratory, Berkeley, CA, USA

<sup>b</sup>Naval Research Laboratory, Washington, DC, USA

## ABSTRACT

We present the design, implementation, and on-ground performance measurements of the Ionospheric Connection Explorer EUV spectrometer, *ICON EUV*, a wide field ( $17^\circ \times 12^\circ$ ) extreme ultraviolet (EUV) imaging spectrograph designed to observe the lower ionosphere at tangent altitudes between 100 and 500 km. The primary targets of the spectrometer, which has a spectral range of 54–88 nm, are the OII emission lines at 61.6 nm and 83.4 nm. Its design, using a single optical element, permits a  $0.25$  imaging resolution perpendicular to the spectral dispersion direction with a large ( $12^\circ$ ) acceptance parallel to the dispersion direction while providing a slit-width dominated spectral resolution of  $R \sim 25$  at 58.4 nm. Pre-flight calibration shows that the instrument has met all of the science performance requirements.

**Keywords:** Extreme Ultraviolet, Instrumentation, Ionosphere, Spectrograph

## 1. INTRODUCTION

The existence of EUV emission from singly ionized oxygen ( $O^+$ ) in the ionosphere of the Earth has long been known and is a useful diagnostic of the ionization state and density of the lower ionosphere.<sup>3</sup> The brightest of the OII dayglow line complexes in the EUV is the 83.4 nm resonance triplet resulting from transition from the  $2p^4\ ^4P$  excited states to the  $2p^3\ ^4S^0$  ground state. The high population of nearby ions in the ground state causes a high probability that an emitted photon from this transition will be reabsorbed, resulting in a high optical depth in this transition. This can make it difficult to disentangle optical depth effects from illumination and ion density effects when attempting to determine density of the  $O^+$  ion. The nearby triplet at 61.6 nm from the  $3s\ ^2P$  state to the  $2p^3\ ^2D^0$  state, is optically thin. In principle, the two taken together can be used to more directly obtain the ion density and illumination source function than the 83.4 nm emission alone.<sup>11</sup> Similar transitions at 67.3 nm and 71.8 nm could be used to supplement this analysis.

---

\*email: sirk@ssl.berkeley.edu

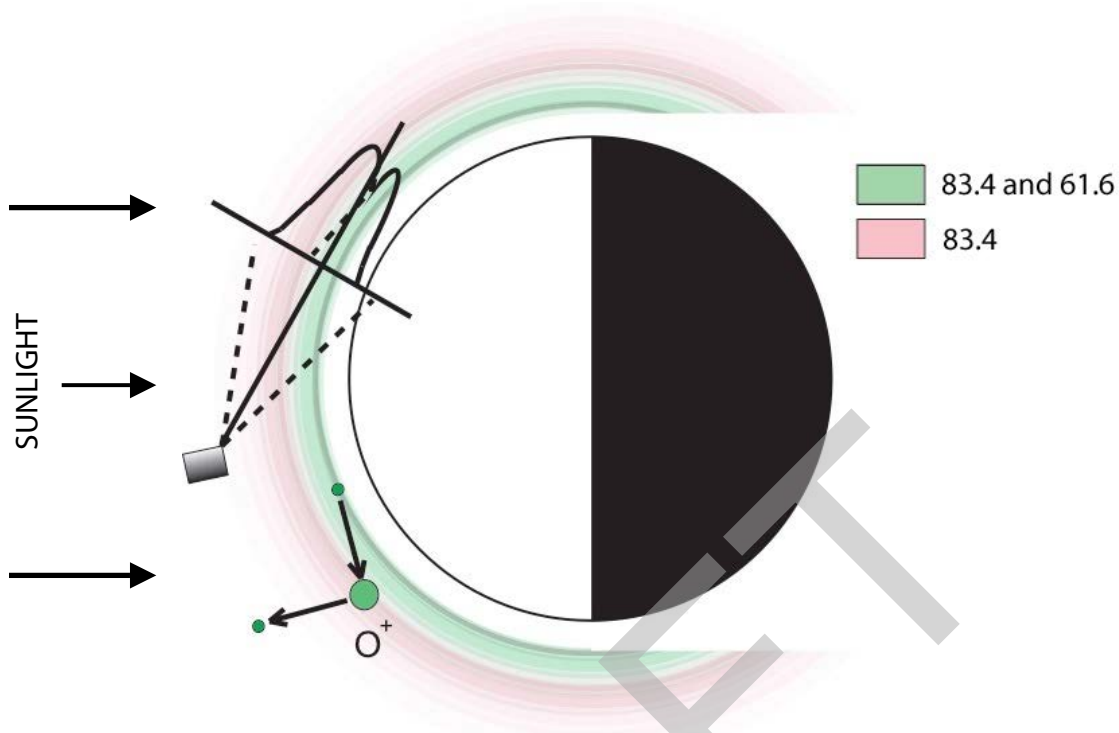


Figure 1. Illustration of the *ICON EUV* observing geometry.

The *ICON EUV* spectrometer has been designed to perform wide field altitude profilometry of the region surrounding the peak  $O^+$  densities in the lower ionosphere, at tangent altitudes between 100 and 500 km (see Figure 1). The primary design requirements relate to obtaining the sensitivity and angular resolution necessary to determine the maximum ion density of the F2 layer and the altitude of the maximum density using the 61.6 nm and 83.4 nm emission while rejecting interference from scattered  $Hi Ly\alpha$  and the nearby  $HeI 58.4$  nm line. Table 1 shows the primary design requirements needed to achieve these goals.

## 2. DESCRIPTION OF INSTRUMENT

The *ICON EUV* instrument is a diffuse imaging spectrograph consisting of an entrance aperture, a diffraction grating, and a microchannel plate (MCP) detector. The grating was manufactured by Horiba Jobin Yvon and delivered with a 40 nm thick coating of Cr. To enhance reflectivity in the EUV additional layers of Ir (20 nm) and  $B_4C$  (10 nm) were applied by Reflective X-ray Optics LLC. The MCP detector and spectrograph were both designed and assembled at the Space Sciences Laboratory (SSL) at the University of California Berkeley Campus. The design is patterned after the successful *SPEAR* mission.<sup>2,7</sup> The spectrograph housing is a hermetic enclosure measuring  $\sim 38$  by 21 by 34 cm and has a mass of 10 kg. Figure 2 is a side view of the instrument including its mounting feet.

Because contamination is a significant concern for EUV instruments, the entire instrument housing is built as a vacuum cavity. A sealed one-shot door in front of the instrument is opened in orbit, or in a vacuum chamber, to allow evacuation and allow light to enter. For ground operations, the instrument

Table 1. *ICON EUV* design requirements

	Requirement	Achieved
Spectral Resolution <sup>a</sup>	4.2 nm	2.4 nm
Angular Imaging Resolution <sup>b</sup>	0°45	0°25
3 $\sigma$ Minimum Measurable Flux <sup>c</sup>		
– at 61.6 nm	<7.4 R	3.3 R (BOL <sup>d</sup> ) 6.6 R (EOL <sup>e</sup> )
– at 83.4 nm	<30 R	3.7 R (BOL) 5.8 R (EOL)
Vertical Field-of-View	>14°	17°3

<sup>a</sup>90% Enclosed Energy Width at 58.4 nm.

<sup>b</sup>Full Width Half Maximum.

<sup>c</sup>in a 60 second exposure.

<sup>d</sup>Beginning of Mission Life.

<sup>e</sup>End of Mission Life (estimated).

can be maintained at high vacuum by attaching a vacuum pump to the instrument’s pumping port. During operations for which pumping is not possible, the instrument can be purged with clean dry nitrogen through a purge port. The purge gas escapes through  $\sim 1$  psi poppet valves that are also used to release pressure during ascent. For short durations, the instrument can be back-filled with dry nitrogen and sealed to prevent contamination.

During operation EUV radiation from the sky enters the 0.9 by 40 mm slit, illuminates a 50 by 95 mm toroidal figure, ion-blazed (lamellar profile), holographically ruled diffraction grating,<sup>9</sup> and is then focused onto a 19 by 54 mm cross delay line MCP detector with a spatial resolution of 90  $\mu\text{m}$  in the spectral direction, and 160  $\mu\text{m}$  in the imaging direction.<sup>1</sup> The field of view is determined by internal and external baffles, and the grating dimensions. The optical scheme provides imaging without using a separate telescope optic. In the spectral direction, the toroid focuses an image of the slit onto the detector while in the imaging direction the toroid focuses at infinity resulting in a spectral image where each row is a horizontal slice of the sky. A diagram of the focusing properties of the grating is shown as Figure 3. The grating is coated with a special EUV-optimized, low stress B4C/Ir/Cr multilayer.<sup>13</sup> The grating parameters are listed in Table 2.

### 3. CALIBRATIONS

The single aperture and single optic simplicity of the instrument inspired this calibration strategy:

1. Separately characterize the performance of the diffraction grating (coating efficiency, order efficiencies) and the detector quantum efficiency (QE) at discrete wavelengths.
2. For the integrated instrument determine the absolute throughput, wavelength scale, resolution, field of view, and in-band, and out-of-band scattering levels at discrete wavelengths.

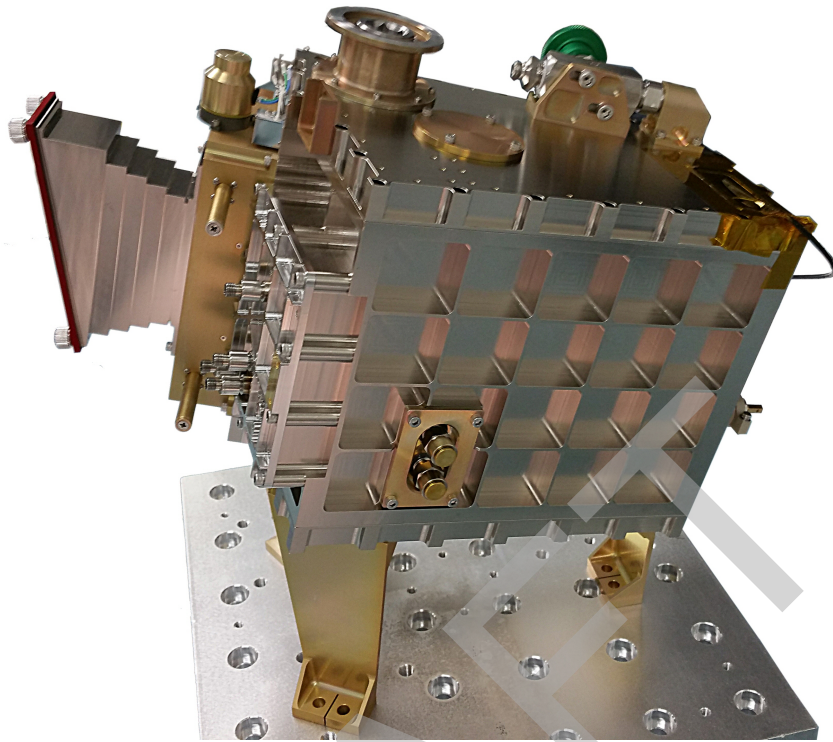


Figure 2. Spectrograph housing. Visible are the external slit baffle at far left, the door mechanism at left (gold), and the MCP detector at near left. One grating adjustment screw is visible at far right. Flight electronics and harnessing are absent.

3. Use efficiency models provided by the diffraction grating and optical coating manufactures that are scaled to SSL measurements to predict performance at other wavelengths.
4. On-orbit, use Moon pointings of reflected Solar EUV light to verify optical alignment, focus, and throughput. Use downward-looking (nadir) pointings to make flat field and vignetting maps.

All calibrations were performed at the SSL vacuum facility. A gas discharge source and monochromator were employed to provide in- and out-of-band, discrete wavelength EUV radiation. A 4-axis manipulator allowed for the testing of both individual components and the complete instrument at various translational and rotational configurations.

Two different modes of illumination were required to fully characterize the optical performance of the spectrograph. Slightly divergent pencil beams (about  $f/150$ ) 1 to 5 mm in diameter proved ideal for field of view and absolute QE determinations. To quantify spectral and spatial resolution required illuminating the entire grating simultaneously. This was accomplished by employing an optical simulator which places a toroidal mirror (with similar radii of curvature as that of the grating) at the foci of the entrance slit and a point source (a spherical mirror illuminated by a collimated pencil beam of EUV light).<sup>5</sup> In effect, the toroidal mirror mimicked a uniformly luminous patch of the sky and focused it as a line  $\approx 0.3$  mm wide along the entrance aperture (slit).

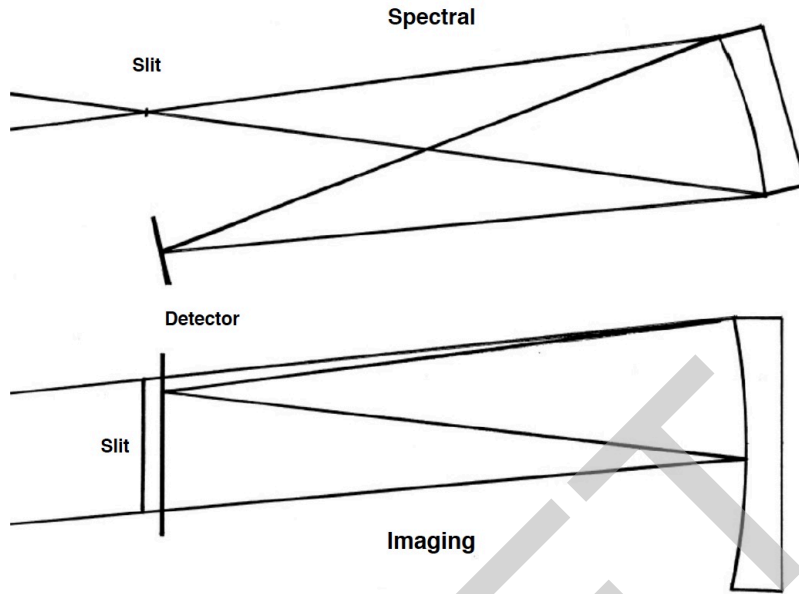


Figure 3. Schematic diagram showing how monochromatic light from the entire 12° wide spectral field of view is directed to one spot on the detector along the dispersion direction (top), and how collimated, in-band light from a particular altitude is focused to one spot on the detector in the imaging direction (bottom).

Table 2. Diffraction grating parameters.

Item	Specification	Notes/Ref.
Grating Substrate	Fused Silica	
Grating Dimensions	100, 55 mm	Imaging, Spectral
Radii of Curvature	335.5, 175.8 mm	Imaging, Spectral <sup>9</sup>
Useful Ruled Area	95 x 50 mm	Ref <sup>9</sup>
Groove Density	3000.28 ±0.2 /mm	Ref <sup>9</sup>
$\alpha_{centralray}$	13°.67	Ref <sup>9</sup>
Cr Thickness	40 nm	Ref <sup>9</sup>
Ir Thickness	20 nm	Ref <sup>13</sup>
B <sub>4</sub> C Thickness	10 nm	Ref <sup>13</sup>
-1 Order	41.75% ±0.19	at 58.4 nm
0 Order	0.81% ±0.066	at 58.4 nm
+1 Order	32.88% ±0.63	at 58.4 nm
+2 Order	1.40% ±0.90	at 58.4 nm

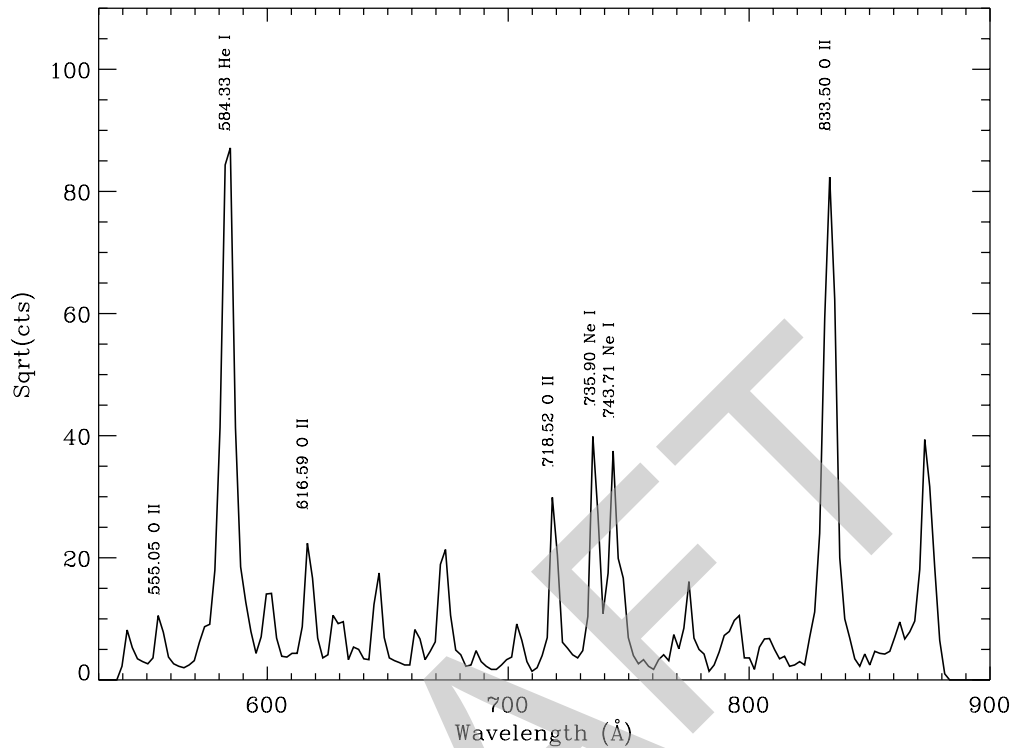


Figure 4. Pencil beam spectra of He-Ne and O. Labeled lines are used for wavelength calibration.

### 3.1 Optical Alignment

Pencil beams of EUV light from He-Ne and O gas discharge were directed through the center of the entrance slit towards the center of the diffraction grating (central ray illumination). Optical alignment was achieved in vacuum by turning the three grating mount fine-adjustment screws via stepper motors while watching the effect on the detector images. Once aligned, seven emission lines were identified and used for a provisional wavelength scale (see Figure 4).

### 3.2 Field of View

The ultimate sensitivity of the instrument at a given wavelength is the product of the instrument throughput efficiency and the etendue (the product of the entrance aperture area and the solid angle of the sky visible by the grating). The slit was measured with a microscope on a fine micrometer stage. The geometrical area is  $0.3616 \pm 0.0016 \text{ cm}^2$ . The angular field of view was determined by shining a pencil beam of EUV light at 3 different positions along the slit while rotating the instrument in both pitch and yaw by known amounts. The field of view is  $17^\circ 31' \pm 0^\circ 1'$  and  $12^\circ 12' \pm 0^\circ 05'$  in the imaging and spectral directions, respectively. This corresponds to a solid angle of  $0.06391 \pm 0.00045 \text{ sr}$ . The

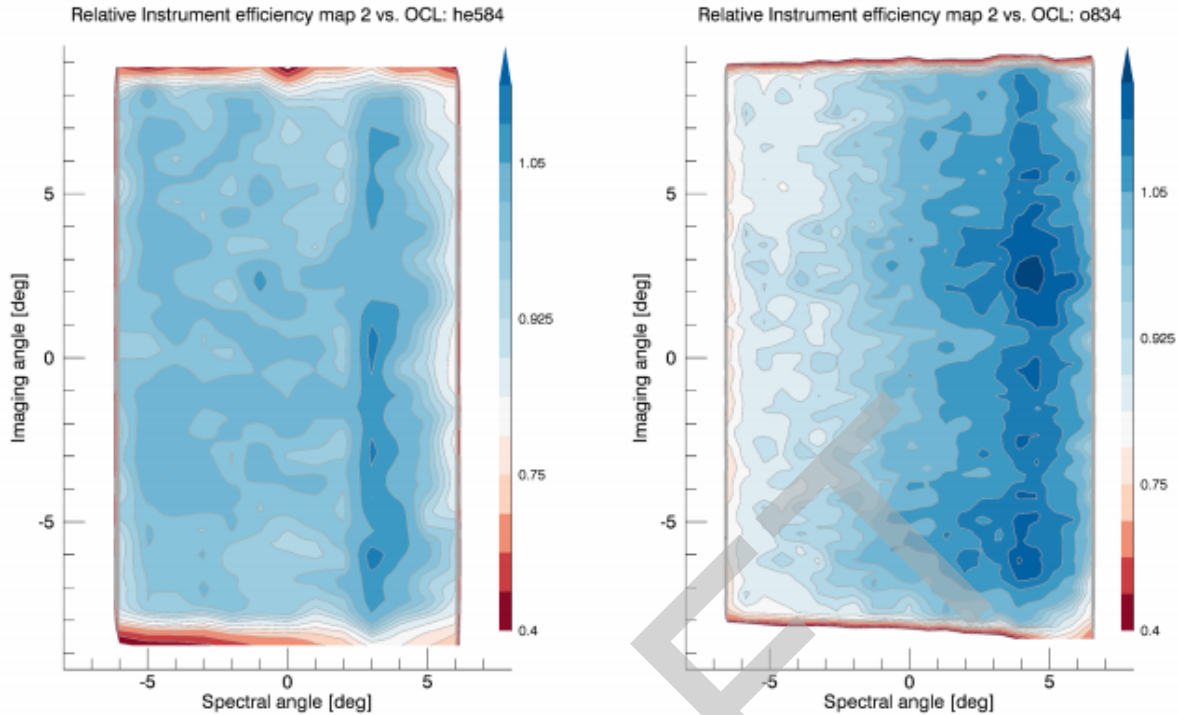


Figure 5. Angular sensitivity maps relative to central ray for 58.4 nm (left) and 83.4 nm (right).

value determined for the imaging direction is for the center of the slit. Off-axis rays may experience vignetting and will be calibrated in orbit using time-averaged nadir pointings.

### 3.3 Absolute Photometric Throughput

The throughput determinations required several steps. First, absolute measurements were performed for the central ray at three wavelengths (58.4, 61.6, and 83.4 nm) by alternately directing pencil beams into the instrument and onto a photodiode calibrated by NIST.<sup>12</sup> To ensure full capture of the EUV pencil beams by the grating, the entrance slit was temporarily removed from the instrument. These measurements provided the absolute photometric sensitivity for on-axis light at the center of the grating.

Second, measurements were made relative to the central ray by rotating and translating the instrument to illuminate the grating at approximately flight-like conditions. In Figure 5 we show the angular response relative to the central ray for both the spectral and imaging angles. The average value of each of these images (excluding regions beyond the measured field of view) gives sensitivities relative to the central ray of 97.8% and 105% at 58.4 nm and 83.4 nm, respectively.

The third step is to determine the sensitivity at other wavelengths. This requires knowing the wavelength dependent efficiencies of the diffraction grating, the  $B_4C/Ir/Cr$  coating, and the flight detector. Measurements were performed for each of these components at discrete wavelengths at SSL. Linear interpolation for intermediate values of detector QE proved adequate. For the coating efficiency and

the grating diffraction order efficiency we use the theoretical performance (based on the measured groove profile) provided by the manufacturers<sup>9,13</sup> and scale these curves to match the Berkeley measurements. We present these in the upper panel of Figure 6. The product of these curves gives the predicted throughput which we compare to the Berkeley measurements in the lower panel of Figure 6.

The predicted instrument efficiency is about 20% greater than the three SSL measurements shown in Figure 6. We investigated these differences using a calibrated reference MCP detector and a second NIST photodiode. The two diodes were measured side by side and agree to within 5%. The instrument responses we determined using the photodiode agreed with those derived from the reference detector to within 11%. We were also careful to account for telemetry losses, detector gain sag, and obscuration of the flight detector from an ion repelling grid. It is likely the higher predicted efficiency is caused by over estimating the reflectivity of the grating coating sample due to an  $\approx 8^\circ$  difference in illumination angle of the reference detector between the through beam and reflected beam configurations. Whatever the cause, we believe that the SSL instrument measurements of throughput are accurate to within an internal uncertainty of 11%.

Accurate knowledge of the uncertainties in the absolute photometric throughput at the wavelengths of interest, namely the OII emission lines at 61.6 nm and 83.4 nm (and, potentially, 67.3 nm and 71.8 nm) is required by the plasma density inversion models. We combine the reference photodiode uncertainty of 7% quoted by NIST<sup>12</sup> and our internal measurement uncertainty of 11% in quadrature to get 13% (the error bars plotted in Figure 6). For throughput at other wavelengths based on interpolations we add an additional error of 5% in quadrature to yield an uncertainty of 14%. These values are our best estimate of the systematic uncertainty in the derived line fluxes.

### 3.4 Spectral and Imaging Resolution

To quantify the focusing properties of the spectrograph required fully illuminating the grating as well as the entrance slit. The optical simulator fully illuminates the grating, but produces a line-image only 1/3 (0.3 mm) as wide as the slit. Hence, small lateral motions of the simulator spherical mirror (slit scans) were required to create synthetic images of a fully illuminated entrance aperture. A set of slit scans obtained at different imaging angles and then added together provides our best proxy for flight-like illumination. In Figure 7 we present the integrated image from the oxygen discharge source.

Combining the synthetic O spectrum with a similar one obtained with He we find a resolution in the imaging direction of  $0''.28$  at FWHM. In the spectral dimension the resolution is slit-limited—emission features appear flat-topped. We find a typical line-width of 2.4 nm at 90% energy width which corresponds to  $R \sim 25$ .

### 3.5 Wavelength Scale

We determine the wavelength scale by using the optical simulator to direct light through the center of the slit. Spectra were obtained with O and He-Ne gases. In the case of blended lines wavelengths are assigned using weighted averages based on values from Kelly and Palumbo.<sup>6</sup> The suitable lines used are identified in Figure 4. A second order polynomial fit is performed to determine wavelength as a function of detector position and shows a RMS residual of  $0.45\text{\AA}$  (0.045 nm). We show the residuals and the dispersion relation in Figure 8.

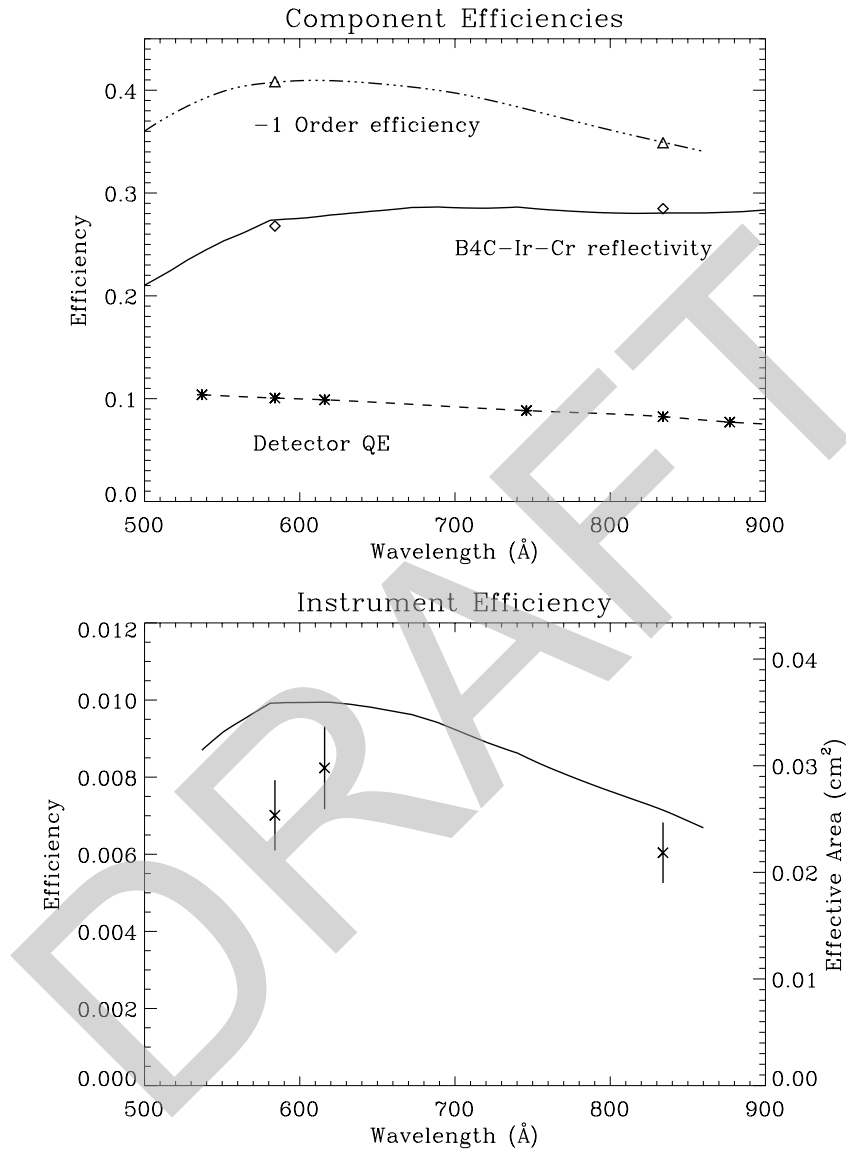


Figure 6. Component (upper) and instrument (lower) efficiencies. The predicted instrument efficiency is the product of the three component curves and is plotted in the lower panel (solid line). In both panels the plotted symbols are the Berkeley measurements. The uncertainties are discussed in the text.

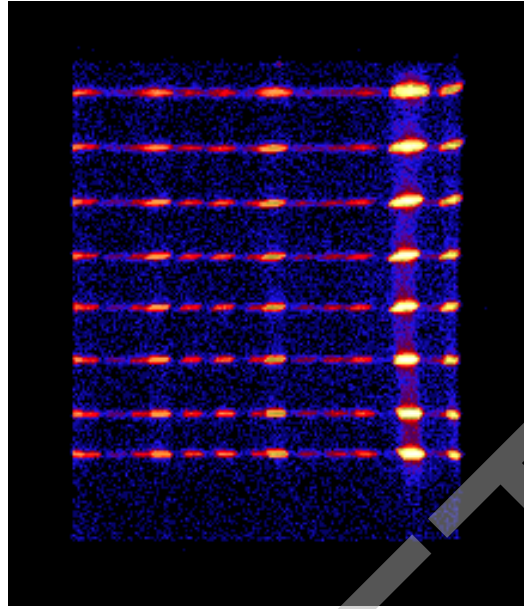


Figure 7. Oxygen spectrum detector image created by adding 8 different slit scans obtained at various image angles. Data have been log-scaled to emphasize faint features. Wavelength increases towards the right as per Figure 4. Brightest feature at right is the OII 83.4 nm emission line.

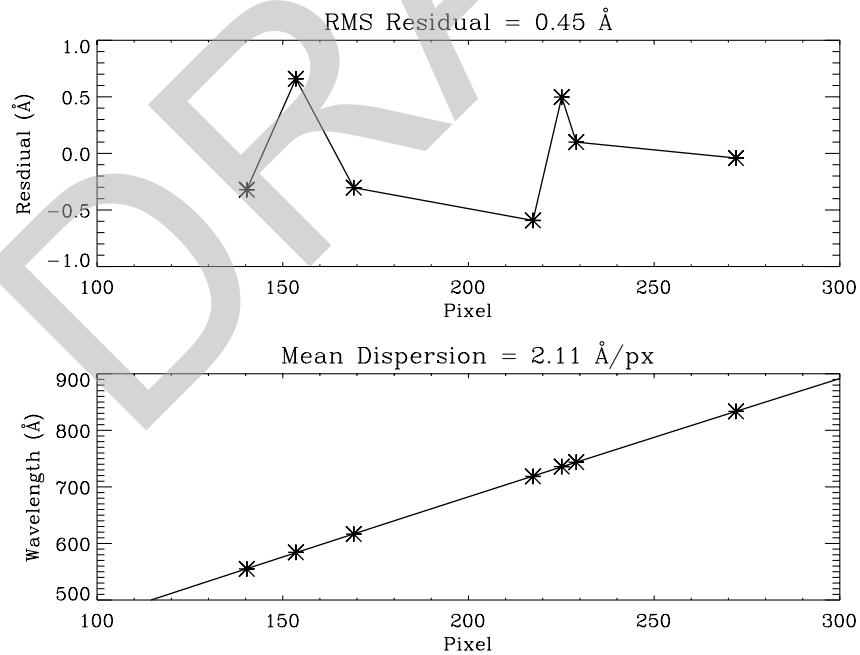


Figure 8. Second order polynomial fit wavelength residual (top) and dispersion relation (bottom).

### 3.6 Scattered and Stray Light

Most spectrographs are compromised to some degree by unwanted light typically caused by the diffraction grating scattering both in-, and out-of-band light, light from orders other than those of interest, and stray light that bounces off one or more interior surfaces and ultimately lands on the detector. When EUV light within the field of view is directed through the *ICON EUV* entrance aperture the holographically ruled gratings with square-wave groove profile<sup>9</sup> shows insignificant ( $< 0.025\%$ ) scattering in-band at 83.4 nm, and out-of-band at 121.6 nm ( $\text{Ly}\alpha$ ). However, when  $\text{Ly}\alpha$  light from beyond the field of view is directed through the aperture it can scatter from one or more baffles directly, or reflect off the grating in several different orders and then scatter from baffles. We measured significant scattering at the detector ( $\approx 19 \text{ cm}^{-2}$  per  $1.5 \times 10^6$   $\text{Ly}\alpha$  input photons) from off-axis light in both the spectral and imaging planes.

Several modifications were required to reduce the scattered light to acceptable levels. In the spectral direction, baffle edges were sharpened to knife edges to prevent glints. Outside of the slit, one baffle was extended slightly to prevent direct illumination of a baffle facet close to the grating. In the imaging direction additional baffles were fabricated to fully shadow existing baffles where knife edging was insufficient. The measured scattering level was reduced by more than a factor of 13 ( $\approx 1.4 \text{ cm}^{-2}$  per  $1.5 \times 10^6$   $\text{Ly}\alpha$  input photons) to a level which should not compromise science observations.

## 4. IN-FLIGHT CALIBRATION

Once in orbit, *ICON EUV* is expected to undergo changes in its spectral response. Anticipated impacts include contamination and reduced gain and count loss due to charge depletion of the microchannel plates in regions of high count rate, primarily near the peak intensity of 83.4 nm. Such changes in instrument response could disrupt the determination of peak ion density and the altitude of peak density. To combat this effect we will be performing two types of in-flight calibrations.

The first will be a monthly recalibration against the full moon. The EUV field of view will be swept across the full moon at seven evenly spaced imaging angles. Using the known EUV albedo of the moon<sup>4</sup> and near-concurrent EUV solar measurements,<sup>10</sup> we will recalculate the spectral response so as to track changes.

The second will be a monthly flat-field calibration. For these calibrations the spacecraft will be oriented so that the EUV instrument boresight is pointing towards nadir with the slit oriented parallel to the spacecraft velocity vector. In this configuration any variation in the atmospheric intensity will quickly traverse along the slit. After a several hundred second exposure, each pixel will have seen essentially the same emitting regions and the resulting image can be used to determine a flat field correction at each of the science wavelengths and imaging angles.

## 5. CONCLUSIONS

The imaging and spectral resolutions are well within specifications. Detector dark background is  $< 0.3 \text{ s}^{-1} \text{ cm}^{-2}$  and therefore negligible. In-band scattering from the grating is also negligible. Out-of-band scattering from  $\text{Ly}\alpha$  has been reduced to levels that should not be problematic. The uniformity in instrument response in the imaging direction (see Figure 5) makes flux determinations straight forward.

The total systematic uncertainty in instrument response is 13% for wavelengths where we have SSL measurements, and 14% for wavelengths which required interpolation.

A set of witness samples that have traveled with the grating or the instrument have had their reflectivity (at 58.4 nm and 83.4 nm) measured periodically. No signs of coating degradation or contamination are evident. The instrument has met all its design requirements.

## ACKNOWLEDGMENTS

We thank Carl Dobson for systems support and Steve Marker who kept the vacuum facility operational. Paul Turin and David Pankow provided useful advice. *ICON* is supported by NASA's Explorers Program through contracts NNG12FA45C and NNG12FA42I. Utilizes data from the NIST Atomic Spectra Database.<sup>8</sup> Special thanks to EUVester the pug.

## REFERENCES

1. Davis, M. W., G. R. Gladstone, T. K. Greathouse, D. C. Slater, M. H. Versteeg, K. B. Persson, G. S. Winters, S. C. Persyn, and J. S. Eterno: 2011, 'Radiometric performance results of the Juno ultraviolet spectrograph (Juno-UVS)'. In: *UV/Optical/IR Space Telescopes and Instruments: Innovative Technologies and Concepts V*, Vol. 8146 of *Proc. SPIE* 814604 doi:10.1117/12.894274
2. Edelstein, J., K.-W. Min, W. Han, E. J. Korpela, K. Nishikida, B. Y. Welsh, C. Heiles, J. Adolfo, M. Bowen, W. M. Feuerstein, K. McKee, J.-T. Lim, K. Ryu, J.-H. Shinn, U.-W. Nam, J.-H. Park, I.-S. Yuk, H. Jin, K.-I. Seon, D.-H. Lee, and E. Sim: 2006, 'The "Spectroscopy of Plasma Evolution from Astrophysical Radiation" Mission'. *Astrophys. J.* **644**, L153–L158 doi:10.1086/505208 arXiv:astro-ph/0601587
3. Feldman, P. D., D. E. Anderson, Jr., R. R. Meier, and E. P. Gentieu: 1981, 'The ultraviolet day-glow. IV - The spectrum and excitation of singly ionized oxygen'. *J. Geophys. Res.* **86**, 3583–3588 doi:10.1029/JA086iA05p03583
4. Flynn, B. C., J. V. Vallerger, G. R. Gladstone, and J. Edelstein: 1998, 'Lunar reflectivity from Extreme Ultraviolet Explorer imaging and spectroscopy of the full moon'. *Geophys. Res. Lett.* **25**, 3253–3256 doi:10.1029/98GL02483
5. Ishikawa, Y., E. Korpela, E. R. Wishnow, M. M. Sirk, J. Curtis, J. McCauley, C. Smith, J. B. McPhate, and J. Edelstein: 2016 (in press), 'Calibration techniques for NASA *ICON* Extreme Ultraviolet Spectrograph (EUV)'. In: *Earth Observing Systems XXI*, Vol. 9972 of *Proc. SPIE* 997245
6. Kelly, R. L. and J. Palumbo: 1973, *NRL Report No. 7599*.
7. Korpela, E. J., J. Edelstein, P. Berg, M. S. Bowen, R. Chung, M. Feuerstein, W. Han, J. S. Hull, H. Jin, D.-h. Lee, K.-w. Min, U.-w. Nam, K. Nishikida, J.-g. Rhee, K. Ryu, K. Seon, B. Y. Welsh, and I. Yuk: 2003, 'The SPEAR science payload'. In: J. C. Blades & O. H. W. Siegmund (ed.): *Future EUV/UV and Visible Space Astrophysics Missions and Instrumentation*, Vol. 4854 of *Proc. SPIE* 665–675 doi:10.1117/12.459970
8. Kramida, A., Y. Ralchenko, J. Reader, and NIST ASD Team: 2015, 'NIST Atomic Spectra Database (version 5.3),[Online]' <http://physics.nist.gov/asd>
9. Liard, A.: 2015, *Final Control Report, Grating 54900269H*. Longjumeau Cedex, France: Horiba Jobin Yvon
10. Pesnell, W. D., B. J. Thompson, and P. C. Chamberlin: 2012, 'The Solar Dynamics Observatory (SDO)'. *Sol. Phys.* **275**, 3–15 doi:10.1007/s11207-011-9841-3

11. Stephan, A. W., J. M. Picone, S. A. Budzien, R. L. Bishop, A. B. Christensen, and J. H. Hecht: 2012, 'Measurement and application of the O II 61.7 nm dayglow'. *J. Geophys. Res. (Space Phys.)* **117**, A01316  
doi:10.1029/2011JA016897
12. Vest, R. E., Y. Barad, M. L. Furst, S. Grantham, C. Tarrío, and P.-S. Shaw: 2006, 'NIST VUV metrology programs to support space-based research'. *Adv. Space Res.* **37**, 283–296  
doi:10.1016/j.asr.2005.02.073
13. Windt, D. L.: 2015, *Private Communication*. New York: Reflective X-ray Optics LLC

DRAFT